PHYSICAL REVIEW D **89,** 123502 (2014)

Black hole universe with a cosmological constant

Chul-Moon Yoo[1,*] and Hirotada Okawa[2,†]

[1]*Gravity and Particle Cosmology Group, Division of Particle and Astrophysical Science, Graduate School of Science, Nagoya University, Nagoya 464-8602, Japan*

[2]*CENTRA, Departamento de Física, Instituto Superior Técnico, Avenida Rovisco Pais no 1, 1049-001 Lisboa, Portugal*

(Received 14 April 2014; published 3 June 2014)

Time evolution of a black hole lattice universe with a positive cosmological constant Λ is simulated. The vacuum Einstein equations are numerically solved in a cubic box with a black hole in the center. Periodic boundary conditions on all pairs of opposite faces are imposed. Configurations of marginally trapped surfaces are analyzed. We describe the time evolution of not only black hole horizons, but also cosmological horizons. Defining the effective scale factor by using the area of a surface of the cubic box, we compare it with that in the spatially flat dust dominated Friedmann-Lemaître-Robertson-Walker (FLRW) universe with the same value of Λ. It is found that the behavior of the effective scale factor is well approximated by that in the FLRW universe. Our result suggests that local inhomogeneities do not significantly affect the global expansion law of the Universe irrespective of the value of Λ.

DOI: 10.1103/PhysRevD.89.123502 PACS numbers: 98.80.Jk

I. INTRODUCTION

The so-called "black hole lattice universe" has been first investigated by Lindquist and Wheeler in 1957 [1]. They regularly arranged N potions of the Schwarzschild spacetime on a virtual three-sphere ($N = 5$, 8, 16, 24, 120 and 600), and discussed the evolution of this lattice universe based on the intuitively derived junction conditions between the Schwarzschild shell and the three-sphere. The black hole lattice universe is often used as one of the tools to evaluate the effects of local nonlinear inhomogeneities on the global expansion. Recently, black hole lattice universe models have been revisited by several authors [2–12]. Time symmetric initial data for N-black hole systems on a virtual three-sphere have been analyzed in Refs. [4,12]. Time evolution of the eight-black hole system has been performed and analyzed in Ref. [7]. Initial data for a black hole inside a cubic box with a periodic boundary condition have been constructed and analyzed in Refs. [3,8], and those time evolutions have been investigated in Refs. [2,7]. We call this cubic lattice model the "black hole universe" in this paper. The purpose of this paper is to extend the black hole universe so that it admits a positive cosmological constant.

In Ref. [2], it has been reported that, if the box size of the black hole universe is sufficiently larger than the horizon radius, the global expansion law can be well approximated by that in the Einstein-de Sitter universe. Our final purpose is to check this fact with a positive cosmological constant. Since our universe is likely to be filled with dark energy components, such as the positive cosmological constant, it is important to investigate the effect of local nonlinear inhomogeneities on the global expansion law with the cosmological constant. In all the references listed above, the cosmological constant is set to be zero. Therefore, solving technical problems to consider nonzero cosmological constant cases, we investigate it in this paper.

One of the nontrivial technical problems is how to construct an initial data set which is appropriate as an initial condition for the time evolution. In this paper, we describe a procedure to construct puncture initial data for the black hole universe with a positive cosmological constant. Another interesting problem is to find different kinds of marginal surfaces. As in the case of the Kottler (Schwarzschild-de Sitter) solution, the black hole universe with a positive cosmological constant can have not only black hole horizons but also de Sitter cosmological horizons. As far as we know, it is the first time to numerically find the $\mathbf{S}^2$ cosmological horizons without any symmetry which makes it possible to reduce the number of the effective dimension. To check the existence and structure of marginal surfaces is very useful to understand the spacetime structure.

This paper is organized as follows. In Sec. II, we describe how to construct initial data of the black hole universe with a positive cosmological constant. Then, we analyze the structure of the initial data in Sec. III searching for different kinds of marginal surfaces. In Sec. IV, time evolutions are described. The evolution of the configuration of marginal surfaces and the expansion law are discussed there. Section V is devoted to a summary.

In this paper, we use the geometrized units in which the speed of light and Newton's gravitational constant are one, respectively.

*yoo@gravity.phys.nagoya-u.ac.jp
†hirotada.okawa@ist.utl.pt

II. INITIAL DATA

A. Constraint equations

Let us consider solutions of vacuum Einstein equations with a positive cosmological constant Λ described by the intrinsic metric γ_{ij} and the extrinsic curvature K_{ij}. The Hamiltonian constraint and the momentum constraint equations are given by

$$\mathcal{R} + K^2 - K_{ij}K^{ij} - 2\Lambda = 0, \tag{1}$$

$$D_j K_i^j - D_i K = 0, \tag{2}$$

where $\mathcal{R}$ and D_i are the Ricci scalar curvature and the covariant derivative with respect to γ_{ij}, and $K = \gamma^{ij}K_{ij}$. We perform conformal decomposition in a conventional way as follows:

$$\gamma_{ij} = \Psi^4 \tilde{\gamma}_{ij}, \tag{3}$$

$$K^{ij} = \Psi^{-10}\left[\tilde{D}^i X^j + \tilde{D}^j X^i - \frac{2}{3}\tilde{\gamma}^{ij}\tilde{D}_k X^k + \hat{A}^{ij}_{\mathrm{TT}}\right] + \frac{1}{3}\Psi^{-4}\tilde{\gamma}^{ij}K, \tag{4}$$

where $\Psi := (\det \gamma_{ij})^{(1/12)}$, $\tilde{D}_i$ is covariant derivative with respect to the conformal metric $\tilde{\gamma}_{ij}$, and $\hat{A}^{ij}_{\mathrm{TT}}$ satisfies

$$\tilde{D}_j \hat{A}^{ij}_{\mathrm{TT}} = 0, \quad \tilde{\gamma}_{ij}\hat{A}^{ij}_{\mathrm{TT}} = 0. \tag{5}$$

To minimize effects of artificial gravitational radiation, we assume

$$\tilde{\gamma}_{ij} = \delta_{ij}, \tag{6}$$

$$\hat{A}^{ij}_{\mathrm{TT}} = 0, \tag{7}$$

where δ_{ij} is the Kronecker's delta. Then, from Eqs. (1) and (2), we obtain

$$\Delta\Psi + \frac{1}{8}(\tilde{L}X)_{ij}(\tilde{L}X)^{ij}\Psi^{-7} - \frac{1}{12}K^2\Psi^5 + \frac{1}{4}\Lambda\Psi^5 = 0, \tag{8}$$

$$\Delta X^i + \frac{1}{3}\partial^i\partial_j X^j - \frac{2}{3}\Psi^6\partial^i K = 0, \tag{9}$$

where

$$(\tilde{L}X)^{ij} := \partial^i X^j + \partial^j X^i - \frac{2}{3}\delta^{ij}\partial_k X^k. \tag{10}$$

First, we need to solve these constraint equations in appropriate settings for puncture initial data with $\Lambda > 0$.

B. Puncture structure with Λ

In this paper, we adopt the Cartesian coordinate system $\boldsymbol{x} = (x, y, z)$. We consider a cubic region $\mathcal{D}$ given by $-L \le x \le L$, $-L \le y \le L$ and $-L \le z \le L$ with periodic boundary conditions on all pairs of faces opposite to each other. Thus, the domain $\mathcal{D}$ is homeomorphic to the three torus $\mathbf{T}^3$. The black hole is represented by a structure like the Einstein-Rosen bridge around the origin $\mathcal{O}(\boldsymbol{x} = 0)$; therefore, the origin corresponds to the asymptotic infinity. The origin $\mathcal{O}$ is often called the "puncture." Since the infinity is not a region of the spacetime, our initial data $\mathcal{D} - \{\mathcal{O}\}$ is homeomorphic to $\mathbf{T}^3$ with one point removed. In the rest of this section, we describe how to construct the puncture initial data with $\Lambda > 0$.

1. Constant mean curvature slice in the Kottler universe

First, we consider a constant mean curvature (CMC) slice in the exact Kottler solution (Schwarzschild-de Sitter) to understand the puncture structure with Λ (see Refs. [13,14] for details of CMC slices in the Kottler solution). Line elements of the Kottler solution are given by

$$ds^2 = -f(r)dt^2 + \frac{1}{f(r)}dr^2 + r^2 d\Omega^2, \tag{11}$$

where

$$f(r) = 1 - \frac{2M}{r} - \frac{\Lambda r^2}{3}. \tag{12}$$

Let us consider a time slice given by

$$t = h(r). \tag{13}$$

The unit normal vector field to this time slice can be expressed as

$$n^\mu = \frac{1}{\sqrt{f^{-1} - fh'^2}}[f^{-1}(\partial_t)^\mu + fh'(\partial_r)^\mu], \tag{14}$$

where $(\partial_t)^\mu$ and $(\partial_r)^\mu$ are coordinate basis vectors. The CMC slice condition with the mean curvature K is given by

$$\begin{aligned}\nabla_\mu n^\mu = -K &\Leftrightarrow \frac{1}{r^2}\partial_r(r^2 n^r) = -K \\ &\Leftarrow n^r = -\frac{1}{3}Kr \\ &\Leftrightarrow f^{-1}(1 - f^2 h'^2) = 1/F(r; M, \Lambda, K) \\ &= \left(1 - \frac{2M}{r} - \frac{1}{3}\Lambda r^2 + \frac{1}{9}K^2 r^2\right)^{-1},\end{aligned} \tag{15}$$

where we have dropped the integration constant and defined $F(r; M, \Lambda, K)$ as

$$F(r; M, \Lambda, K) := \left(1 - \frac{2M}{r} - \frac{1}{3}\Lambda r^2 + \frac{1}{9}K^2 r^2\right). \tag{16}$$

The induced metric on the time slice is given by

$$d\ell^2 = F(r; M, \Lambda, K)^{-1}dr^2 + r^2 d\Omega^2. \tag{17}$$

Transformation to the isotropic coordinate can be performed as follows:

$$d\ell^2 = \Psi^4(dR^2 + R^2 d\Omega^2), \tag{18}$$

$$R = C\exp\left[\pm\int_{r_{\min}}^{r}\frac{dr}{r\sqrt{F(r;M,\Lambda,K)}}\right], \tag{19}$$

$$\Psi = \sqrt{r/R}, \tag{20}$$

where $r_{\min}$ is the throat radius given by $F(r_{\min};M,\Lambda,K)=0$. The minus sign branch is used in the region inside the throat. For this branch, the puncture structure requires

$$R = 0 \quad \text{for } r\to\infty. \tag{21}$$

This requirement can be satisfied by setting

$$K^2 = 3\Lambda. \tag{22}$$

This implies that we need to impose this condition near the origin of the numerical box. Under this condition, the conformal factor Ψ is given by

$$\Psi = 1 + \frac{M}{2R}, \tag{23}$$

where we have set the integration constant C as $C = M/2$ to fix the mass of the black hole measured in the infinity inside the black hole as M (see Ref. [3]).

2. Form of K and the asymptotic solution near the origin

In this paper, we adopt the following form of K:

$$K(\boldsymbol{x}) = K_\Lambda + (K_{\rm b} - K_\Lambda)W(R), \tag{24}$$

where $R:=|\boldsymbol{x}|$, $K_\Lambda = -\sqrt{3\Lambda}$, and

$$W(R) = \begin{cases} 0 & \text{for } 0 \le R \le \ell \\ \sigma^{-36}[(R-\sigma-\ell)^6 - \sigma^6]^6 & \text{for } \ell \le R \le \ell+\sigma \\ 1 & \text{for } \ell+\sigma \le R \end{cases}. \tag{25}$$

$K_{\rm b}$ is a constant determined by an integrability condition discussed below. We set $\ell = 0.1M$ and $\sigma = L - 0.2M$. The asymptotic solution near the center is given by

$$X^i \simeq 0, \tag{26}$$

$$\Psi \simeq 1 + \frac{M}{2R}. \tag{27}$$

To extract the $1/R$ divergence, we define a new variable ψ as follows:

$$\psi(\boldsymbol{x}) := \Psi(\boldsymbol{x}) - \frac{M}{2R}[1 - W(R)]. \tag{28}$$

Then, the Hamiltonian constraint becomes

$$\Delta\psi = \Delta\left(\frac{M}{2R}W(R)\right) - \frac{1}{8}(\tilde{L}X)_{ij}(\tilde{L}X)^{ij}\Psi^{-7} + \frac{1}{12}K^2\Psi^5 - \frac{1}{4}\Lambda\Psi^5. \tag{29}$$

3. Integrability condition and equations

Integrating Eq. (8) over the physical domain $\mathcal{D}-\{O\}$, we obtain the following equation:

$$2\pi M + \frac{1}{8}\int_{\mathcal{D}-\{O\}}(\tilde{L}X)_{ij}(\tilde{L}X)^{ij}\Psi^{-7}dx^3 - \frac{1}{12}(V_1K_{\rm b}^2 + 2V_2K_\Lambda K_{\rm b} - V_3K_\Lambda^2) = 0, \tag{30}$$

where

$$V_1 := \int_{\mathcal{D}-\{O\}} W^2\Psi^5 d^3x, \tag{31}$$

$$V_2 := \int_{\mathcal{D}-\{O\}} (1-W)W\Psi^5 d^3x, \tag{32}$$

$$V_3 := V_1 + 2V_2. \tag{33}$$

This equation is the integrability condition and we choose the value of $K_{\rm b}$ so that Eq. (30) is satisfied. That is, $K_{\rm b}$ cannot be freely chosen but it must be appropriately fixed through the numerical iteration.

Introducing Z defined by

$$Z := \partial_i X^i, \tag{34}$$

we can derive the following coupled elliptic equations:

$$\Delta\psi = \Delta\left(\frac{M}{2R}W(R)\right) - \frac{1}{8}(\tilde{L}X)_{ij}(\tilde{L}X)^{ij}\Psi^{-7} + \frac{1}{12}K^2\Psi^5 - \frac{1}{4}\Lambda\Psi^5,$$

$$\Delta Z = \frac{1}{2}\partial_i(\Psi^6\partial^i K),$$

$$\Delta X^i = -\frac{1}{3}\partial^i Z + \frac{2}{3}\Psi^6\partial^i K.$$

We solve these equations by using the same procedure described in Ref. [3].

III. MARGINAL SURFACES

As is explicitly shown below, in our initial data, there are four marginal surfaces at most: two cosmological horizons (CHs) and two white hole horizons (WHs) or black hole horizons (BHs), if the cosmological constant is smaller than the Nariai bound $\Lambda = 1/(9M^2)$ [15,16]. We focus on $\Lambda < 1/(9M^2)$ cases in this paper.

Hereafter, we use the words "inner," "outer," "ingoing," and "outgoing" based on the value of the numerical coordinate $\boldsymbol{x}$. That is, the innermost region is near the puncture and outermost region is near the boundary of the numerical box.

The expansions of the future directed null vector fields normal to a two surface are given by

$$\chi_{\pm} = (\gamma^{ij} - s^i s^j)(\pm D_i s_j - K_{ij}), \tag{35}$$

where s^i is the outgoing unit vector on the initial hypersurface which is normal to the two surface. The subscript "+" means outgoing and "−" means ingoing null expansion. If the initial hypersurface is passing through a black hole region as in the case $\Lambda = 0$ [3], there are two black hole horizons (future outer trapping horizons in terms of Ref. [17]). In this case, the outer black hole horizon (OBH) satisfies $\chi_+ = 0$, and the inner black hole horizon (IBH) satisfies $\chi_- = 0$. If the initial hypersurface is passing through a white hole region, two white hole horizons (past outer trapping) exist. In this case, the outer white hole horizon (OWH) satisfies $\chi_- = 0$, and the inner white hole horizon (IWH) satisfies $\chi_+ = 0$. In addition, we have cosmological horizons(past inner trapping). The inner cosmological horizon (ICH) satisfying $\chi_+ = 0$ always exists inside IBH or IWH, although we may not always find it due to the low resolution of numerical grids. If the box size L is sufficiently large and $1/(9M^2) > \Lambda > 0$, we can find the outer cosmological horizon (OCH) satisfying $\chi_- = 0$ outside OBH or OWH.

Equations for marginal surfaces can be rewritten as

$$\chi_+ = 0 \Leftrightarrow D_i s^i - K + K_{ij} s^i s^j = 0 \quad \text{for IWH(OBH) and ICH,} \tag{36}$$

$$\chi_- = 0 \Leftrightarrow D_i s^i + K - K_{ij} s^i s^j = 0 \quad \text{for OWH(IBH) and OCH.} \tag{37}$$

Assuming that the marginal surfaces are expressed by $R = h(\vartheta, \varphi)$ in the spherical coordinate, we can rewrite Eqs. (36) and (37) as

$$\frac{\partial^2 h}{\partial \vartheta^2} + \cot\vartheta \frac{\partial h}{\partial \vartheta} + \frac{1}{\sin^2\vartheta} \frac{\partial^2 h}{\partial \varphi^2} - (2-\eta)h = \eta h + S_{\pm}(h), \tag{38}$$

where η is a constant and $S_{\pm}$ is a complicated function of h and geometric quantities (see e.g. [18]). We set $\eta = 3$ for CHs and $\eta = 1$ for WHs (BHs). Although the reason is not clear, our experience shows that if we set $\eta = 1$ ($\eta = 3$), we cannot find CHs (BHs and WHs) irrespective of the initial trial for the iteration [19].

In our settings, we may find four kinds of possible horizon configurations. For each case, existing horizons can be listed from inside to outside as follows:

(a) ICH, IWH, OWH
(b) ICH, IWH, OWH, OCH
(c) ICH, IBH, OBH
(d) ICH, IBH, OBH, OCH

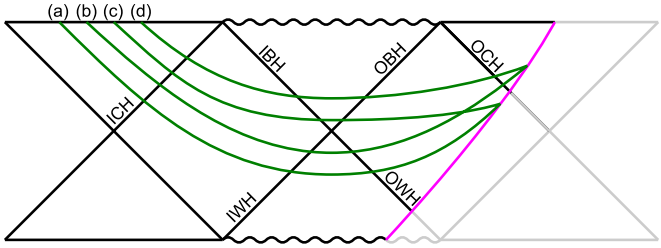

FIG. 1 (color online). Possible hypersurface configurations.

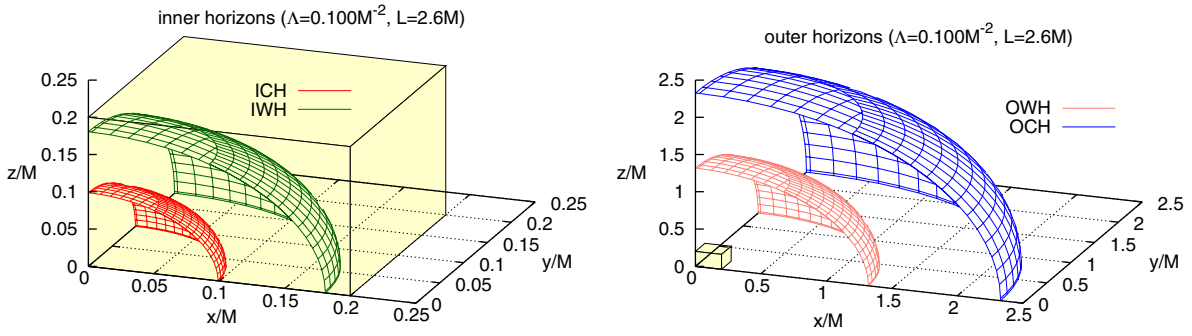

FIG. 2 (color online). Inner (left) and outer (right) marginal surfaces with $\Lambda = 0.1/M^2$, $L = 2.6M$. The left panel is a closeup figure of the central part of the right panel. This configuration is classified in case (b).

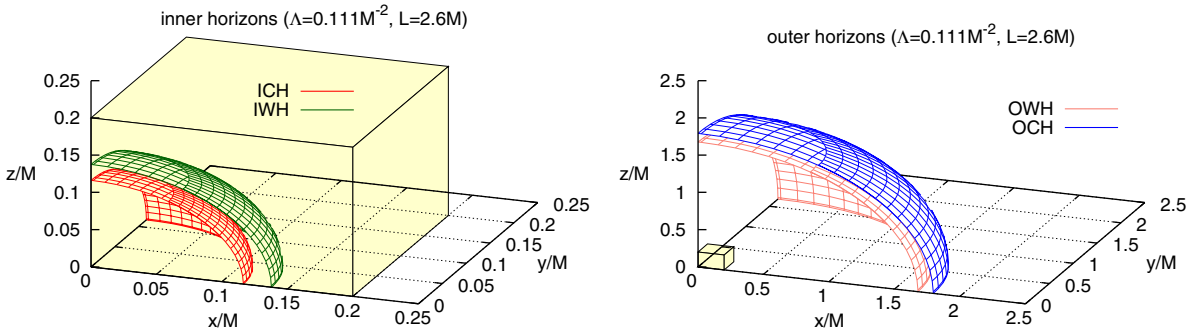

FIG. 3 (color online). Inner (left) and outer (right) marginal surfaces with $\Lambda = 0.111/M^2$, $L = 2.6M$. The left panel is a closeup figure of the central part of the right panel. This configuration is classified in case (b).

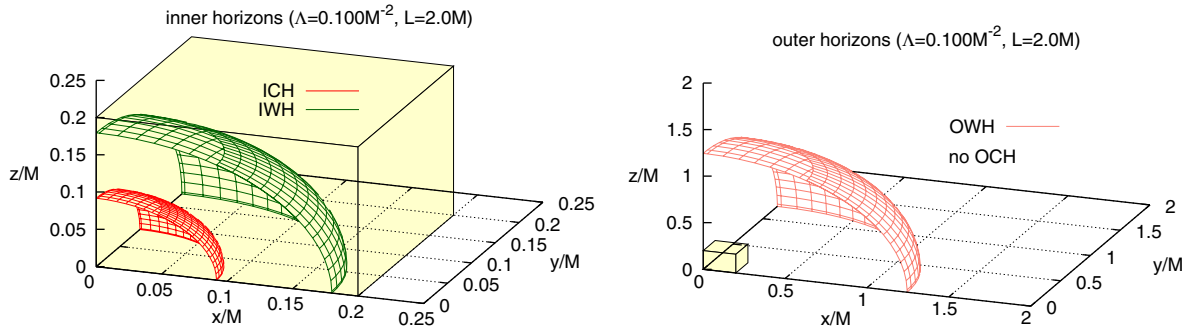

FIG. 4 (color online). Inner (left) and outer (right) marginal surfaces with $\Lambda = 0.1/M^2$, $L = 2M$. The left panel is a closeup figure of the central part of the right panel. This configuration is classified in case (a).

To understand these configurations, it is convenient to consider the Carter-Penrose diagram of the Kottler solution with an outside portion removed. A schematic figure of possible configurations is described in Fig. 1.

We briefly show the configuration of marginal surfaces on initial hypersurfaces. We note that, differently from the $\Lambda = 0$ case in Ref. [3], the hypersurface may pass through the white hole region for a sufficiently large value of Λ. In this subsection, we only show the cases in which the hypersurface is passing through the white hole region, that is, cases (a) or (b). As is shown in Fig. 2, there are four marginal surfaces for $\Lambda = 0.1/M^2$ and $L = 2.6M$. If we increase the value of Λ to $0.111/M^2$, two pairs of WHs and CHs get closer as shown in Fig. 3 and all marginal surfaces disappear for $\Lambda > 1/(9M^2)$. If we decrease the value of L to $2M$, OCH disappears as is shown in Fig. 4.

IV. TIME EVOLUTION

A. Settings and constraint violation

We solve the following evolution equations by using the Baumgarte-Shapiro-Shibata-Nakamura (BSSN) formalism [20,21]:

$$\frac{\partial \gamma_{ij}}{\partial t} = -2K_{ij}, \tag{39}$$

$$\frac{\partial K_{ij}}{\partial t} = R_{ij} + KK_{ij} - 2K_{ik}K^k_j - \Lambda\gamma_{ij}. \tag{40}$$

We describe line elements of the spacetime as follows:

$$ds^2 = -N^2dt^2 + \gamma_{ij}(dx^i + \beta^i dt)(dx^j + \beta^j dt). \tag{41}$$

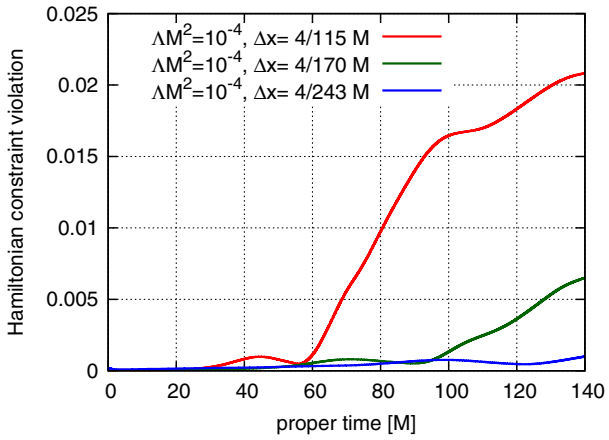

FIG. 5 (color online). Time evolution of the L1 norm of the Hamiltonian constraint violation. The value is appropriately normalized so that the minimum and maximum values are zero and one, respectively.

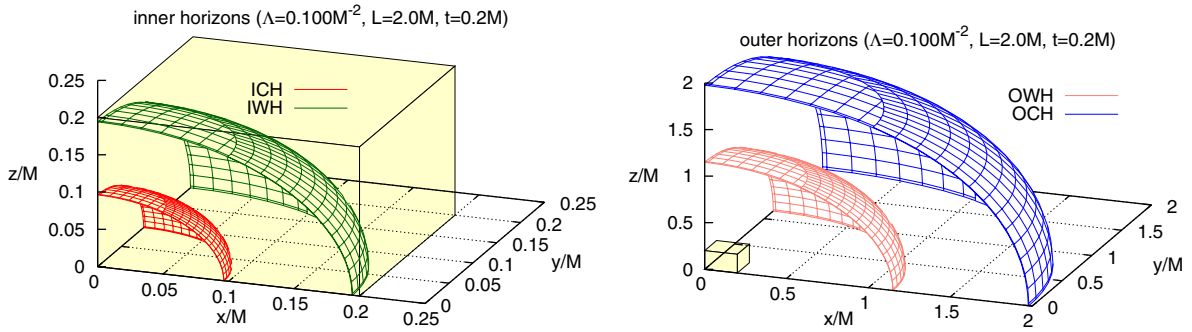

FIG. 6 (color online). Inner (left) and outer (right) marginal surfaces with $\Lambda = 0.1/M^2$, $L = 2M$ on the time slice given by $t \sim 0.2M$. The left panel is a closeup figure of the central part of the right panel. This configuration is classified in case (b).

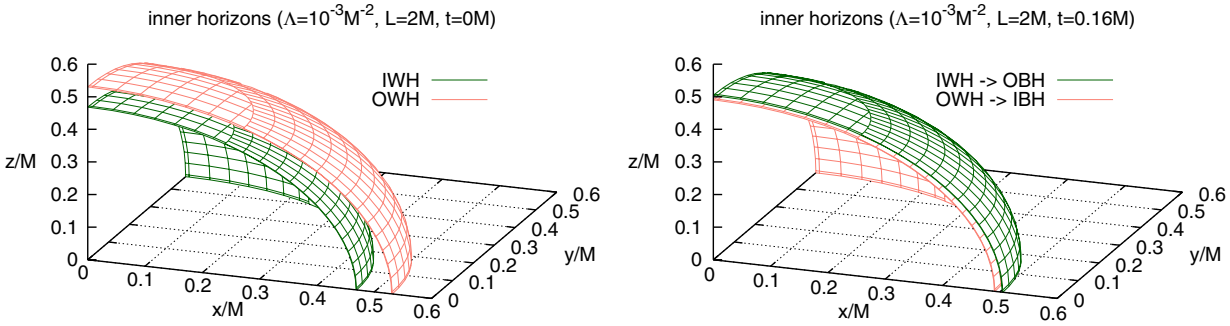

FIG. 7 (color online). For $\Lambda = 10^{-3}/M^2$ and $L = 2M$, the initial hypersurface is passing through the white hole region and these marginal surfaces are WHs (left). After the time evolution, the time slice crosses the bifurcation two surface and the marginal surfaces become BHs (right). Note that, while IWH and OBH satisfy $\chi_+ = 0$, OWH and IBH satisfy $\chi_- = 0$.

Following the previous paper [2], we use the following gauge conditions:

$$\left(\frac{\partial}{\partial t} - \beta^i \frac{\partial}{\partial x^i}\right) N = -2N(K - K_c), \tag{42}$$

$$\frac{\partial \beta^i}{\partial t} = B^i, \tag{43}$$

$$\frac{\partial B^i}{\partial t} = \frac{\partial \tilde{\Gamma}^i}{\partial t} - \frac{3}{4M} B^i, \tag{44}$$

where $\tilde{\Gamma}^i := -\partial_j \tilde{\gamma}^{ij}$ and K_c is the value of K at the vertex of the box.

Numerical simulations are performed with the coordinate grid intervals $\Delta x/M = 4/51$, $4/115$, $4/179$, and $4/243$. The convergence of the Hamiltonian constraint violation is demonstrated in Fig. 5 for the case of $\Lambda = 10^{-4}/M^2$. We also show the convergence of the expansion law defining an effective scale factor in Sec. IV C.

B. Evolution of marginal surfaces

1. Appearance of OCH

One typical example ($\Lambda = 0.1/M^2$ and $L = 2M$) is shown in Fig. 6. As is shown in Fig. 4 there is no OCH for this case at the initial time. After the time evolution, at a

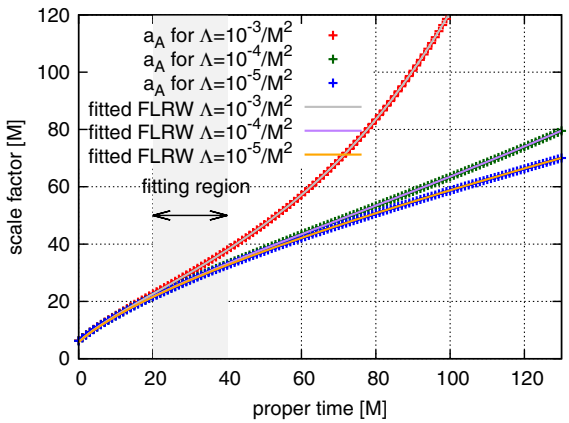

FIG. 8 (color online). Effective scale factors and a_{FLRW} for $\Lambda = 10^{-3}/M^2, 10^{-4}/M^2$, and $10^{-5}/M^2$, where we set $\Delta x = 4/179$.

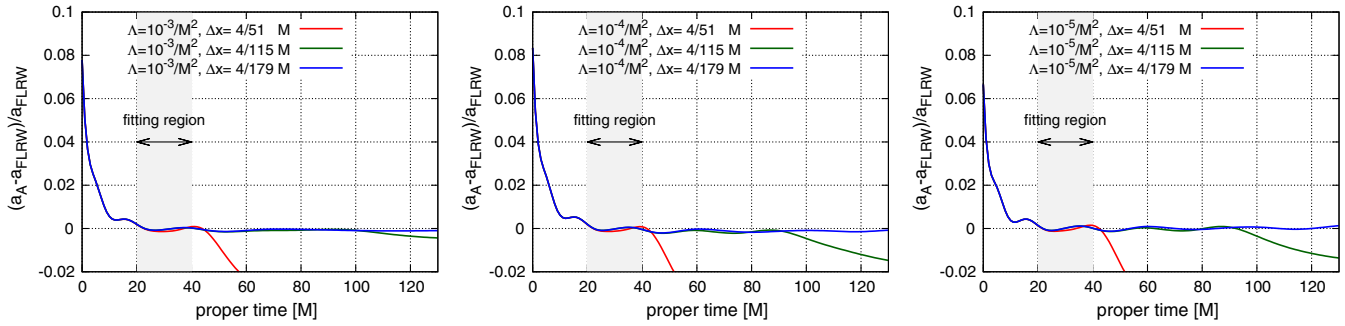

FIG. 9 (color online). Deviation of the effective scale factors from $a_{\rm FLRW}$. We also show the convergence of the result with smaller grid intervals in this figure.

time $t \sim 0.2M$, the OCH appears near the boundary of the box. That is, the horizon configuration can change from case (a) to case (b) through time evolution (see. Fig. 1).

2. Bifurcation surface crossing

The other typical example is the bifurcation surface crossing. As is shown in Fig. 7, for $\Lambda = 10^{-3}/M^2$ and $L = 2M$, IWH ($\chi_+ = 0$) exists outside OWH ($\chi_- = 0$). After the time evolution, at the time $t \sim 0.15M$, the surface satisfying $\chi_+ = 0$ comes out outside the surface satisfying $\chi_- = 0$. This implies that the hypersurface is passing through the black hole region and those surfaces are BHs. That is, the transitions from (a) to (c) or from (b) to (d) may happen through time evolution.

C. Cosmic expansion

We obtain the geodesic slices parametrized by the proper time τ by using the same procedure described in Ref. [2]. Then, we calculate the effective scale factor defined by

$$a_{\mathcal{A}} := \sqrt{\mathcal{A}(\tau)}, \tag{45}$$

where $\mathcal{A}$ is the proper area of a surface on the geodesic slice. On the other hand, the scale factor for flat dust Friedmann-Lemaître-Robertson-Walker (FLRW) with Λ can be written as

$$a_{\rm FLRW} = a_{\rm f}\left[\frac{(1-\exp[\sqrt{3\Lambda}(t+t_{\rm f})])^2}{(1+\exp[\sqrt{3\Lambda}(t+t_{\rm f})])^2-(1-\exp[\sqrt{3\Lambda}(t+t_{\rm f})])^2}\right]^{1/3}, \tag{46}$$

TABLE I. The fitted values for $t_{\rm f}$ and $a_{\rm f}$.

ΛM^2	10^{-3}	10^{-4}	10^{-5}
$t_{\rm f}$	$3.29M$	$3.21M$	$3.18M$
$a_{\rm f}$	$29.2M$	$62.8M$	$135.3M$

where we have two free parameters $t_{\rm f}$ and $a_{\rm f}$. We fix these parameters by fitting this form to results of numerical calculation.

Results are shown in Figs. 8 and 9. Here, the evolution of the effective scale factor is fitted by $a_{\rm FLRW}$. The fitted values for $t_{\rm f}$ and $a_{\rm f}$ are listed in Table I. In Fig. 9, we show the deviation of the effective scale factors from $a_{\rm FLRW}$. This figure explicitly shows that, if the box size of the black hole universe is sufficiently larger than the horizon radius, the global expansion law can be well approximated by a corresponding flat dust FLRW universe irrespective of the value of the positive cosmological constant. We also show the convergence of the result with smaller grid intervals in Fig. 9.

V. SUMMARY

In this work, a black hole lattice universe model with a positive cosmological constant has been simulated. The construction of puncture initial data with a positive cosmological constant has been described in Sec. II. The vacuum Einstein equations in a cubic box with a black hole in the center have been numerically solved with periodic boundary conditions by using the BSSN formalism [20,21]. Configurations of marginal surfaces on the initial hypersurfaces and those time evolution have been analyzed. We found two impressive transitions of the configuration in time evolution: the appearance of the outer cosmological horizon and the bifurcation surface crossing. Finally, comparing the effective scale factor defined by the surface area and the scale factor for the corresponding flat dust FLRW universe, we have concluded that the expansion law of the black hole universe can be well approximated by that of the corresponding flat dust FLRW universe in the sufficiently late time irrespective of the value of the cosmological constant.

ACKNOWLEDGMENTS

We thank T. Tanaka, M. Sasaki, and K. Nakao for helpful discussions and comments.

[1] R. W. Lindquist and J. A. Wheeler, Rev. Mod. Phys. **29**, 432 (1957).
[2] C.-M. Yoo, H. Okawa, and K.-i. Nakao, Phys. Rev. Lett. **111**, 161102 (2013).
[3] C.-M. Yoo, H. Abe, K.-i. Nakao, and Y. Takamori, Phys. Rev. D **86**, 044027 (2012).
[4] T. Clifton, K. Rosquist, and R. Tavakol, Phys. Rev. D **86**, 043506 (2012).
[5] T. Clifton and P. G. Ferreira, Phys. Rev. D **80**, 103503 (2009).
[6] J.-P. Uzan, G. F. Ellis, and J. Larena, Gen. Relativ. Gravit. **43**, 191 (2011).
[7] E. Bentivegna and M. Korzynski, Classical Quantum Gravity **29**, 165007 (2012).
[8] E. Bentivegna, Classical Quantum Gravity **31**, 035004 (2014).
[9] J.-P. Bruneton and J. Larena, Classical Quantum Gravity **29**, 155001 (2012).
[10] T. Clifton, D. Gregoris, K. Rosquist, and R. Tavakol, J. Cosmol. Astropart. Phys. 11 (2013) 010.
[11] T. Clifton, D. Gregoris, and K. Rosquist, Classical Quantum Gravity **31**, 105012 (2014).
[12] M. Korzyński, Classical Quantum Gravity **31**, 085002 (2014).
[13] R. Beig and J. M. Heinzle, Commun. Math. Phys. **260**, 673 (2005).
[14] K.-I. Nakao, K.-I. Maeda, T. Nakamura, and K.-I. Oohara, Phys. Rev. D **44**, 1326 (1991).
[15] H. Nariai, Sci. Rep. Tohoku Univ. Eighth Ser. **34**, 160 (1950).
[16] H. Nariai, Gen. Relativ. Gravit. **31**, 963 (1999).
[17] S. Hayward, Phys. Rev. D **49**, 6467 (1994).
[18] M. Shibata, Phys. Rev. D **55**, 2002 (1997).
[19] K.-I. Nakao (private communication).
[20] M. Shibata and T. Nakamura, Phys. Rev. D **52**, 5428 (1995).
[21] T. W. Baumgarte and S. L. Shapiro, Phys. Rev. D **59**, 024007 (1999).